ORGANIC PROCESS RESEARCH & DEVELOPMENT
OPR&D

pubs.acs.org/OPRD

Article

Citral-to-Menthol Transformations in a Continuous Reactor over Ni/Mesoporous Aluminosilicate Extrudates Containing a Sepiolite Clay Binder

Irina L. Simakova, Zuzana Vajglová, Päivi Mäki-Arvela, Kari Eränen, Leena Hupa, Markus Peurla, Ermei M. Mäkilä, Johan Wärnå, and Dmitry Yu. Murzin*

Cite This: *Org. Process Res. Dev.* 2022, 26, 387−403

Read Online

ACCESS | Metrics & More | Article Recommendations | Supporting Information

ABSTRACT: One-pot continuous synthesis of menthols from citral was performed over 5 wt % Ni supported on a mesoporous aluminosilicate catalyst with sepiolite as a binder at 70 °C with a selectivity of 75% to menthols. Catalyst deactivation with time-on-stream resulted in a decrease of the conversion and selectivity to menthols at the expense of higher selectivity to isopulegols. Stereoselectivity to isopulegols and menthols only slightly changed with conversion and TOS. A kinetic model capable of describing experimental data for transformations of citral to menthol in a continuous mode was developed. It was based on a detailed reaction network and also comprised deactivation on both metal and acid sites. Numerical data fitting confirmed a good correspondence between the experimental data and calculations.

KEYWORDS: *citral, menthol, shaped Ni catalyst, clay binder, trickle-bed reactor*

Downloaded via UNIV OF TURKU on April 22, 2022 at 05:59:25 (UTC).
See https://pubs.acs.org/sharingguidelines for options on how to legitimately share published articles.

INTRODUCTION

Production of menthol, a compound with local anesthetic and counterirritant properties, acting also as a weak k-opiod receptor agonist, has attracted significant attention because of its physiological behavior. Menthol, occurring naturally in peppermint oil, can be manufactured by freezing this oil followed by filtration of menthol crystals. Substantial amounts of menthol are also produced by synthetic routes starting from renewable sources. Manufacturing of menthol from myrcene starts with formation of an allylic amine, followed by asymmetric isomerization using a BINAP rhodium complex giving enantiomerically pure cintronellal after hydrolysis.[1] Subsequent steps include cyclization to isopulegol and hydrogenation to menthol. This route has been commercialized by Takasago International Corporation.[2] An alternative route involves *m*-cresol, which is alkylated with propene to form thymol.[3] The latter is hydrogenated over heterogeneous catalysts resulting in a mixture of menthol enantiomers,[4−8] which are separated by chiral resolution. A particular interesting option is the one-pot synthesis of menthol starting from another renewable source, citral. The latter is obtained by distillation of essential oils.

As can be seen from Figure 1, citral comprises three functional groups, which can be hydrogenated on metal sites. Selective hydrogenation of the double bond adjacent to the carbonyl groups gives cintronellal[9,10] on the metal sites. This reaction should be selective not resulting in hydrogenation of either the second double bond or the carbonyl group to citronellol[10] and further to 3,7-dimethyloctanol. Cyclization of citronellal to isopulegol requires an acidic catalyst.[11,12] The final step in this reaction path is hydrogenation of isopulegol.[13]

Several reports are available in the literature on one-pot citral transformations in batch reactors.[14−20] High yields of menthol (94%) were obtained starting from citral at 70 °C and 20 bar hydrogen over 8 wt % Ni/Al-H-MCM-41 and 15 wt % Ni-MCM-41-Zr-β.[14,16] Mäki-Arvela et al. reported that the selectivity of 54% to four stereoisomers of menthols was achieved at 100% citral conversion over 15 wt % Ni-H-MCM-41 under 10 bar total pressure at 70 °C in cyclohexane.[19] The stereoselective ratio of (±)-menthols/(±)-neomenthols/(±)-isomenthols was 71:25:4% with the absence of (±)-neo-isomenthols in the reaction mixture.[19] Noble metals, such as Pd, Pt, or Ru, have also been applied in a quest for a delicate balance between hydrogenation ability of the catalyst and its acidity.[15−20] These active metals could lead to overhydrogenation, while too acidic catalysts can give rise to dehydration and defunctionalized products. In addition to nickel, other nonnoble metals, including, for example, copper,[21] supported on a natural material sepiolite of the following structure $Si_{12}O_{30}Mg_8(OH)_4(OH_2)_4 8H_2O$,[22] gave 45% menthol yield in heptane at 90 °C under 1 bar hydrogen in a batch reactor.[21]

In our recent work, we have reported mildly acidic mesoporous Ru-MCM-41 with a relatively large size of ruthenium clusters for one-pot synthesis of menthol from citral in batch and continuous reactors.[20] Such a large size (7−20 nm) was intended to diminish the hydrogenation activity. The catalyst along with microporous Ru-H-Y-80 was not very

Received: November 16, 2021
Published: January 25, 2022

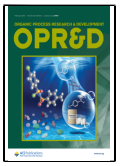

ACS Publications

© 2022 The Authors. Published by American Chemical Society

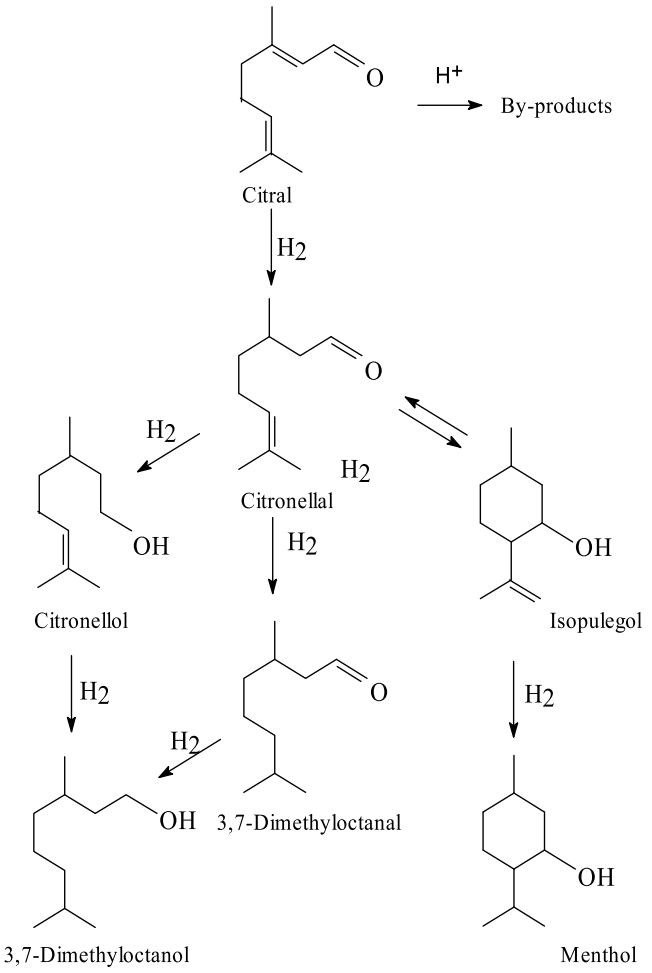

Figure 1. Transformations of citral to menthol.

selective toward menthol, giving defunctionalized menthatrienes as the main products.[23]

Continuous menthol production from citronellal requires utilization of either shaped catalyst bodies or structured reactors to avoid high pressure drop, inevitable with powder catalysts.[24] In a series of studies, various aspects of catalyst shaping by their extrusion and utilization for menthol production have been addressed, including selection of the binder (e.g., bentonite or Ludox) and the metal location using Ru as the main metal.[20,23,25−27] Based on this previous experience, sepiolite was selected as the binder, Ni as a metal for hydrogenation, and a mildly acidic mesoporous aluminosilicate as a metal support and simultaneously, an acid catalyst for citronellal cyclization. Ni/MCM-41 catalysts have been previously demonstrated as rather selective for one-pot synthesis of menthol from citral in a batch reactor.[14,16,17,19] It should, however, be mentioned that catalyst shaping with an inorganic binder, which itself can be selective, for example, in cyclization, can influence catalytic performance of the final extrudate influencing not only activity, but more importantly selectivity to the desired products.

As mentioned above, there are only a handful of papers in the literature where one-pot continuous transformations of citral to menthol have been reported. None of them consider any kinetic analysis or discuss catalyst deactivation in a quantitative way. In fact, the open literature is devoid of kinetic analysis of such one-pot transformations even for experimental data generated in a batch mode. Thus, the aim of this work was not only to study performance of a nickel catalyst supported on a mesoporous aluminosilicate in a continuous mode but also to develop a kinetic model of this process, which will include deactivation of the bifunctional catalyst.

RESULTS AND DISCUSSION

Characterization of Ni Catalysts. Nickel supported on mesoporous aluminosilicate catalysts was characterized before and after the reaction by inductively coupled plasma-optical emission spectrometry (ICP-OES), transmission electron microscopy (TEM), nitrogen physisorption technique, X-ray diffraction method (XRD), scanning electron microscopy with energy-dispersive X-ray microanalysis (SEM-EDX), Fourier transform infrared spectroscopy (FTIR), and crush testing.

Nickel loading and particle size as well as some textural data for Ni supported on mesoporous aluminosilicate catalysts are presented in Table 1. Isotherms and pore size distribution of catalysts are shown in Figures S1 and S2.

According to ICP-OES analysis (Table 1) of the fresh reduced and spent Ni catalysts, nickel loading decreased during citral transformations regardless of the operation mode (batch or continuous). The nickel content in the powder Ni/MAS catalyst decreased from 4.76 to 4.55%, while for the extruded catalyst it changed from 6.30 to 5.95%, supposedly due to insignificant metal leaching during citral conversion (Table 1).

The sorption isotherm of catalysts is of type IV according to IUPAC classification (Figure S1a). Characteristic features of the Type IV isotherm are its hysteresis loop, which is associated with capillary condensation taking place in mesopores and the limiting uptake over a range of high $p/p°$.[28] A type H2 hysteresis loop indicated that the samples are mesoporous materials with cage-like mesopores formed due to disordered blocked pore shapes.[28] Prior to the reaction, the fresh reduced powder Ni/MAS catalyst exhibited a specific surface area (S_{BET}) of 447 m^2/g and total pore volume (V) of 0.47 cm^3/g (Table 1). After citral conversion, the surface area and pore volume of the catalyst decreased to 280 m^2/g (S_{BET}) and 0.36 cm^3/g, respectively (Table 1 and Figure S1a). The same trend was also noticed for

Table 1. Concentration and Particle Size of Nickel and Textural Properties of the Catalysts[a]

catalyst	[Ni] (wt %)	d_{Ni} (XRD) (nm)	d_{Ni} (TEM) (nm)	S_{BET} (m^2/g)	S_{D-R} (m^2/g)	V (cm^2/g)	V_m (%)
fresh, reduced powder Ni/MAS	4.76		8	447	412	0.47	71.1
spent, powder Ni/MAS	4.55		13	280	317	0.36	66.3
fresh, reduced crushed extrudates Ni/(MAS + sepiolite)	6.30		12	743	756	0.85	71.0
fresh, reduced extrudates Ni/(MAS + sepiolite)				337	329	0.39	75.5
spent, extrudates Ni/(MAS + sepiolite)	5.95	11	14	149	214	0.31	81.0

[a][Ni]—concentration of Ni determined by ICP-OES, d_{Ni} (XRD)—average particle size of Ni determined by XRD, d_{Ni} (TEM)—median particle size of Ni determined by TEM, S—specific surface area calculated by BET and Dubinin−Radushkevich equations, V—total pore volume (micro + mesopore volume) calculated by the density functional theory (DFT) method, and V_m—percentage of the mesopore volume.

https://doi.org/10.1021/acs.oprd.1c00435
Org. Process Res. Dev. 2022, 26, 387−403

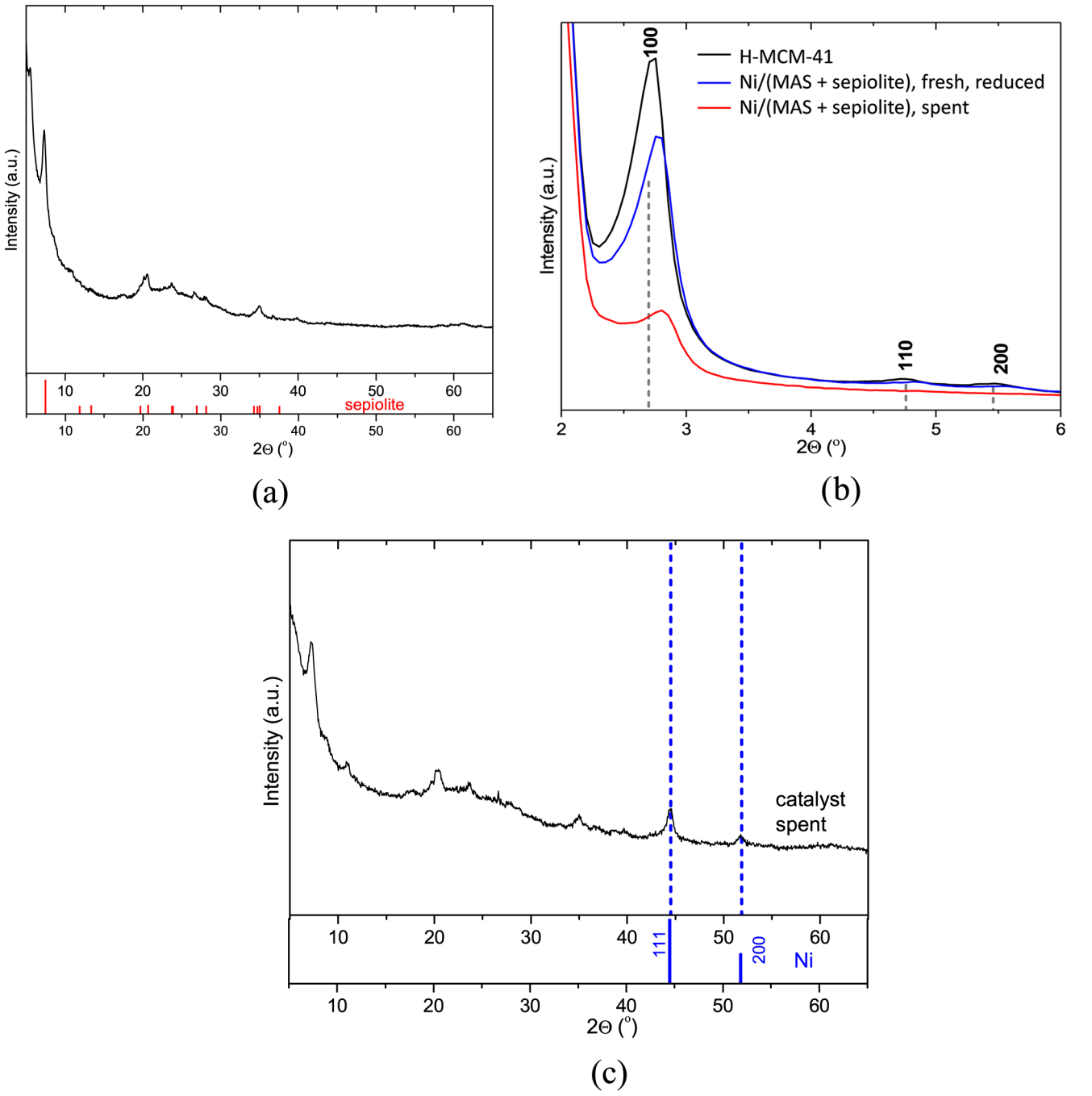

Figure 2. XRD patterns of (a) fresh reduced extrudates, with sepiolite reflections marked in red, (b) support (black) and freshly reduced Ni-containing (blue) and spent (red) extrudate samples at low angle, and (c) spent extrudates.

the extrudates during citral transformations in the continuous reactor under the same reaction conditions giving a decrease of the surface area from 337 to 149 m^2/g (S_{BET}) and pore volume from 0.39 to 0.31 cm^3/g (V) (Table 1 and Figure S1b). A lower surface area and pore volume of Ni/(MAS + sepiolite) extrudates compared to powder Ni/MAS catalysts can be assigned to sepiolite that clogged pores of the pristine aluminosilicate during extrusion. Interestingly, crushing of the fresh reduced extrudates Ni/(MAS + sepiolite) significantly increased the surface area from 337 to 743 m^2/g (S_{BET}), indicating that the groud catalyst is able to expose much more available sites for N_2 molecule adsorption. All samples exhibited more than 66% of the mesopore volume. After the reaction, the fraction of the mesopore volume of extrudates increased; however, the total pore volume decreased, which can be explained by preferential blocking of micropores in line with pore size distribution (Figure S2).

Pristine support along with the fresh reduced and spent extrudates (Figure 2) as well as powdered Ni/MAS catalyst (fresh calcined, fresh reduced, and spent samples) (Figure S3) were studied by powder X-ray diffraction (XRD).

The observed lines indicated the presence of sepiolite phase $Mg_4Si_6O_{15}(OH)_2(H_2O)_6$ (PDF # 04-014-4557) (Figure 2a). XRD patterns of the studied materials at low angles showed that the positions and intensities of the observed diffraction lines correspond to the MCM-41 material (Figure 2b).[29] The

https://doi.org/10.1021/acs.oprd.1c00435
Org. Process Res. Dev. 2022, 26, 387−403

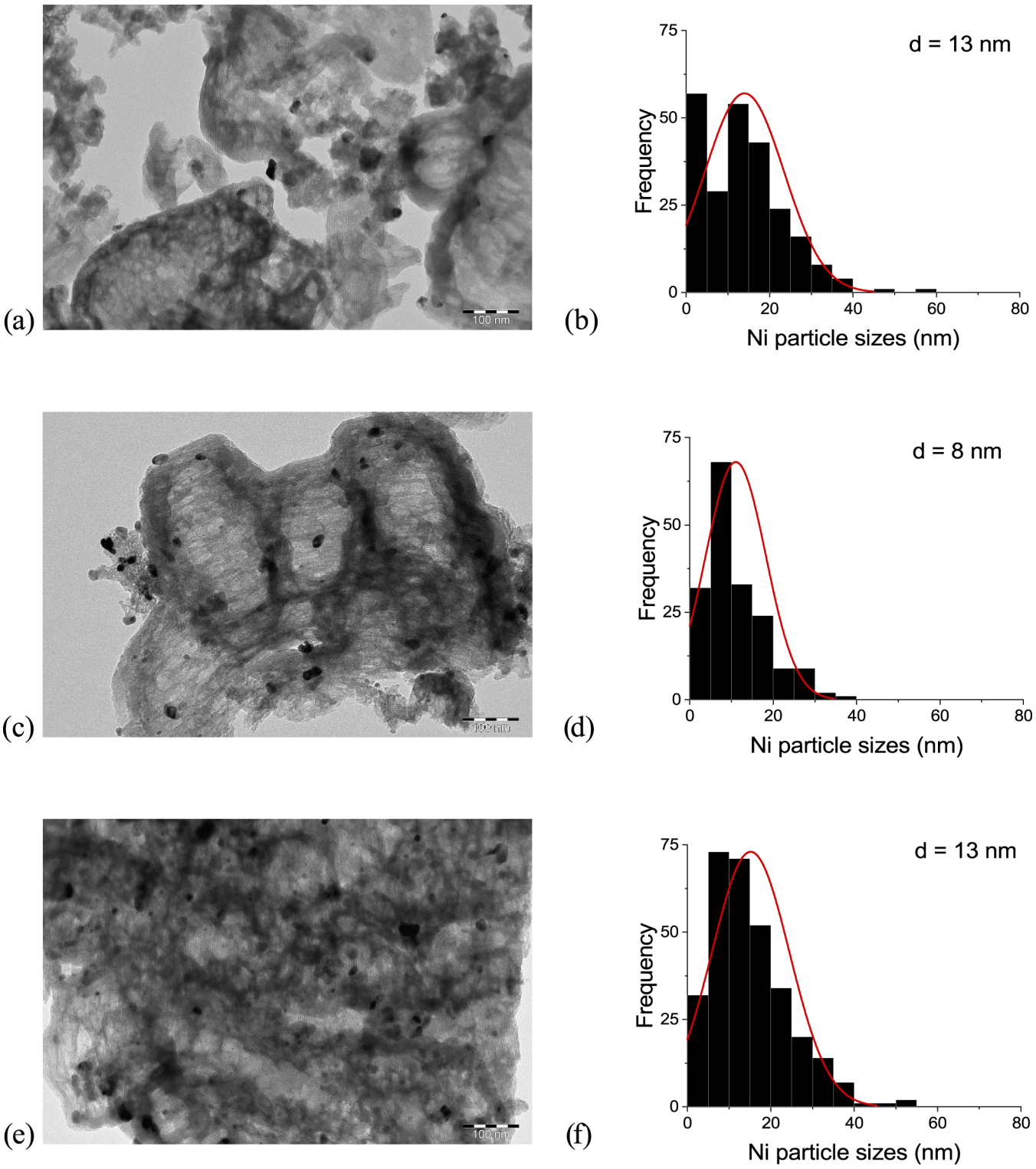

Figure 3. continued

https://doi.org/10.1021/acs.oprd.1c00435
Org. Process Res. Dev. 2022, 26, 387−403

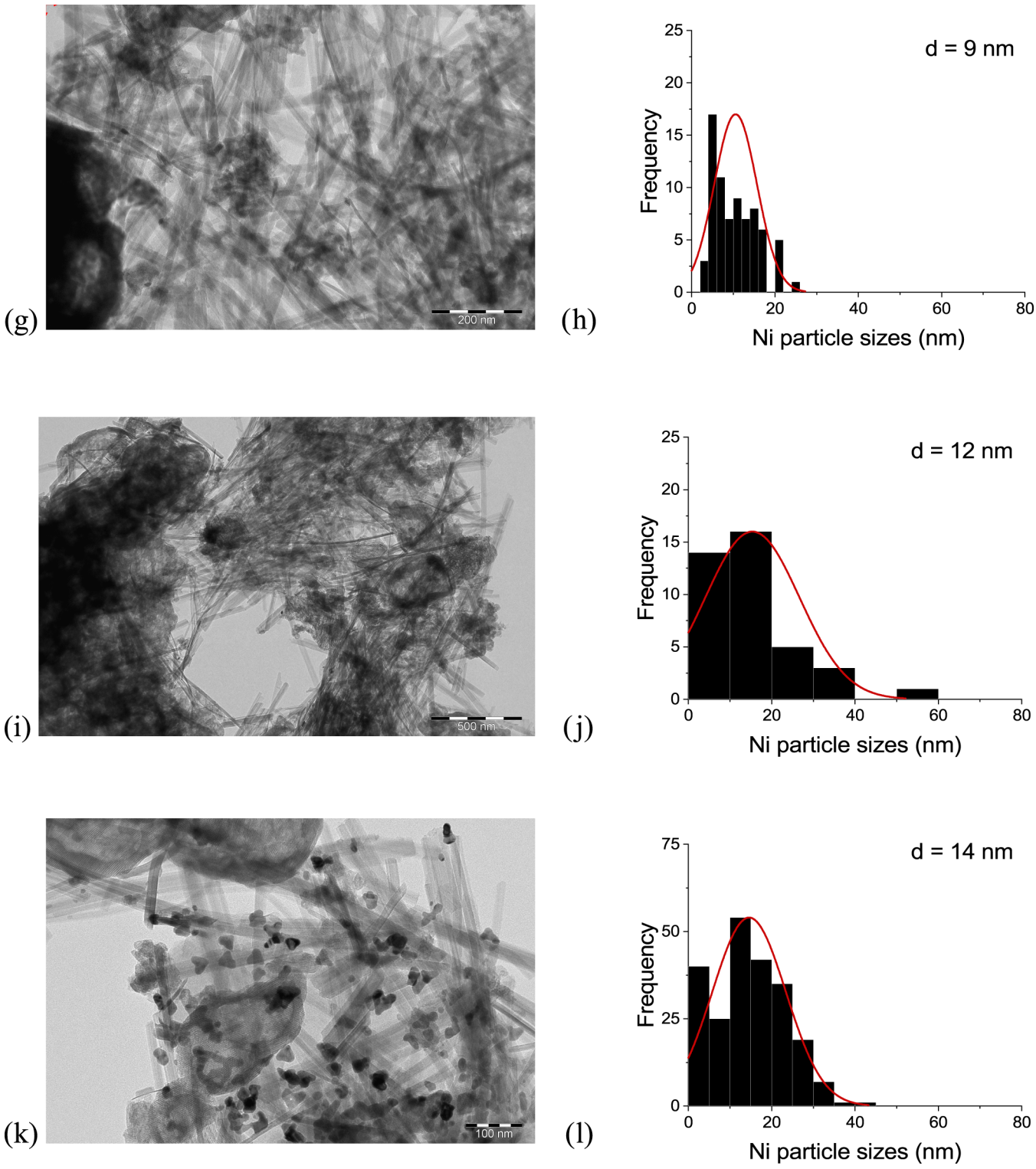

Figure 3. TEM images and Ni particle size distribution: (a, b) Ni/MAS fresh nonreduced powder catalyst, (c, d) Ni/MAS fresh reduced powder catalyst, (e, f) Ni/MAS spent powder catalyst, (g, h) Ni/(MAS + sepiolite) fresh nonreduced extrudates, (i, j) Ni/(MAS + sepiolite) fresh reduced extrudates, and (k, l) Ni/(MAS + sepiolite) spent extrudates.

interplanar distances d_{100} for the mesoporous support, freshly reduced, and spent extrudates were respectively 32.4, 31.8, and 31.5 Å. The corresponding values of the hexagonal lattice parameter defined as $2d_{100}/\sqrt{3}$ were 37.4, 36.7, and 36.4 Å. A significant decrease in the reflections for the spent catalyst compared to the MCM-41 phase can be associated with more prominent structural disordering after the reaction (Figure 2b).

XRD patterns of the spent extrudates are presented in Figure 2c. Along with the lines from sepiolite phase $Mg_4Si_6O_{15}(OH)_2(H_2O)_6$, the lines from the metallic nickel Ni^0 phase (PDF No. 04-0850) are presented. The average coherent scattering domain size (CSD) of Ni^0 D_{Ni} is 11.0 nm that is consistent with TEM data (Table 1 and Figure 3l). The determined value of the Ni lattice parameter a = 3.524 Å. Note

https://doi.org/10.1021/acs.oprd.1c00435
Org. Process Res. Dev. 2022, 26, 387−403

Table 2. Brønsted and Lewis Acid Sites of Ni/MAS Fresh Nonreduced Powder Catalyst[a]

catalyst	BAS				LAS				TAS	B/L
	w	m	s	Σ	w	m	s	Σ	μmol/g	
H-MCM-41[27]	41	19	24	84	20	14	21	56	140	1.5
fresh, reduced powder Ni/MAS	18	25	9	51	35	13	7	55	106	0.9
fresh, reduced extrudates Ni/(MAS + sepiolite)	23	7	0	30	24	11	0	35	65	0.9

[a]BAS—Brønsted acid sites; LAS—Lewis acid sites; TAS—total acid sites; s—strong acid sites, data at 450 °C; m—medium acid sites, data at 350 °C minus data at 450 °C; and w—weak acid sites, data at 250 °C minus data at 350 °C; and B/L—ratio of Brønsted-to-Lewis acid sites.

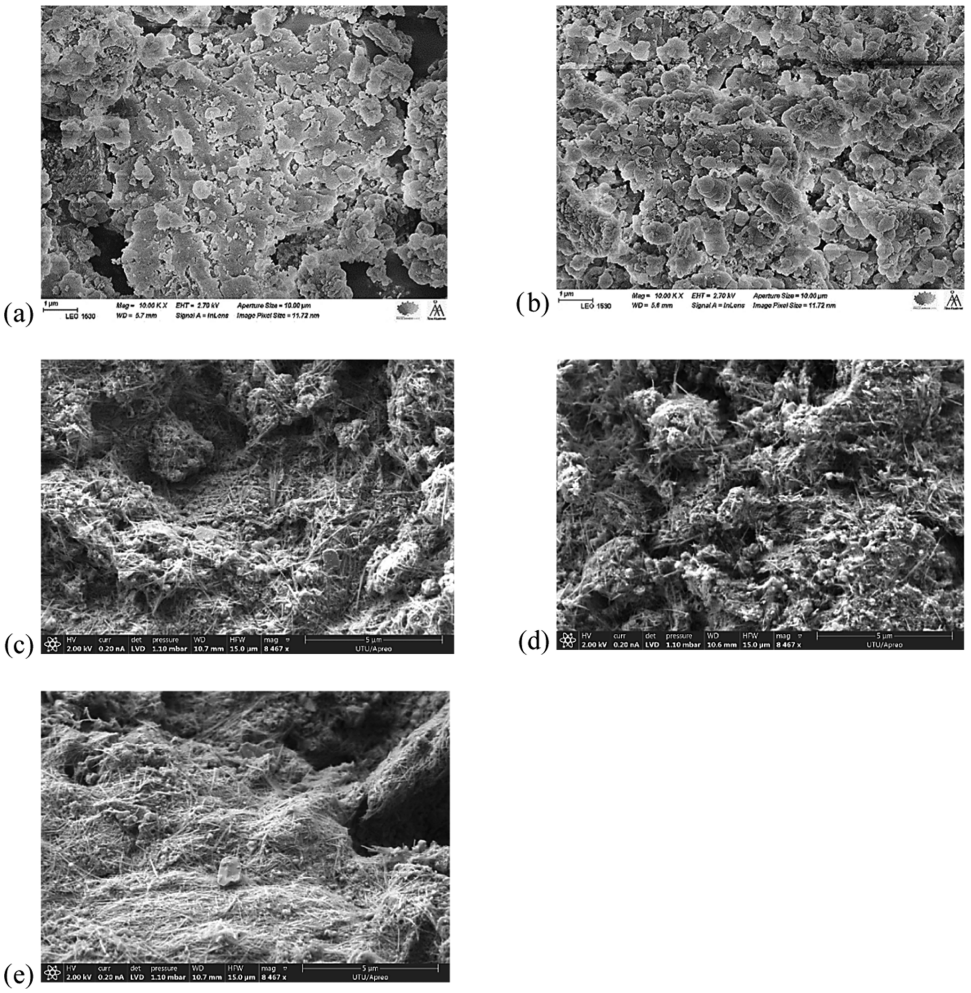

Figure 4. SEM images: (a) Ni/MAS fresh nonreduced powder catalyst, (b) Ni/MAS fresh reduced powder catalyst, (c) Ni/(MAS + sepiolite) fresh nonreduced extrudates, (d) Ni/(MAS + sepiolite) fresh reduced extrudates, and (e) Ni/(MAS + sepiolite) spent extrudates.

there are no additional lines in XRD patterns of the fresh reduced and spent catalysts other than characteristic lines of MCM-41, indicating stability of the support texture after deposition of nickel and subsequent treatment as well as upon exposure to the reaction media.

The irregular shape of Ni particles was observed for all Ni catalysts by TEM analysis (Figure 3). The median Ni particle size for the fresh and spent powder Ni/H-MCM-41 catalyst without a binder was the same, 13 nm, with a broad range from 0.2 to 56 nm. TEM analysis of Ni extrudates clearly confirmed that Ni was deposited randomly on both H-MCM-41 and the sepiolite binder. The median Ni particle size was 9 nm for the fresh extrudates. This value is smaller than that for the powder catalyst without a binder and can be attributed to the impact of extrusion *per se* and the additional thermal treatment after shaping being similar to previous observations for Pt extrudates.[30] Such a behavior was explained by variations in the location of metal particles on the support and the binder, and the influence of the organic binder methylcellulose. The latter, upon calcination, is removed acting as a reducing agent for metal particles, thereby increasing the metal dispersion by forming small metal particles.[30] On the contrary, a slightly larger median Ni particle size of 14 nm for the spent extrudates, compared to the fresh extrudates, can be an indication of minor agglomeration.

FTIR results for the Ni/MAS fresh nonreduced powder catalyst and Ni/(MAS + sepiolite) fresh reduced extrudates are reported in Table 2 together with the pristine H-MCM-41[27] powder catalyst for comparison. A slightly higher value of weak Lewis acid sites, 35 μmol/g, but lower total acid sites and lower

https://doi.org/10.1021/acs.oprd.1c00435
Org. Process Res. Dev. 2022, 26, 387−403

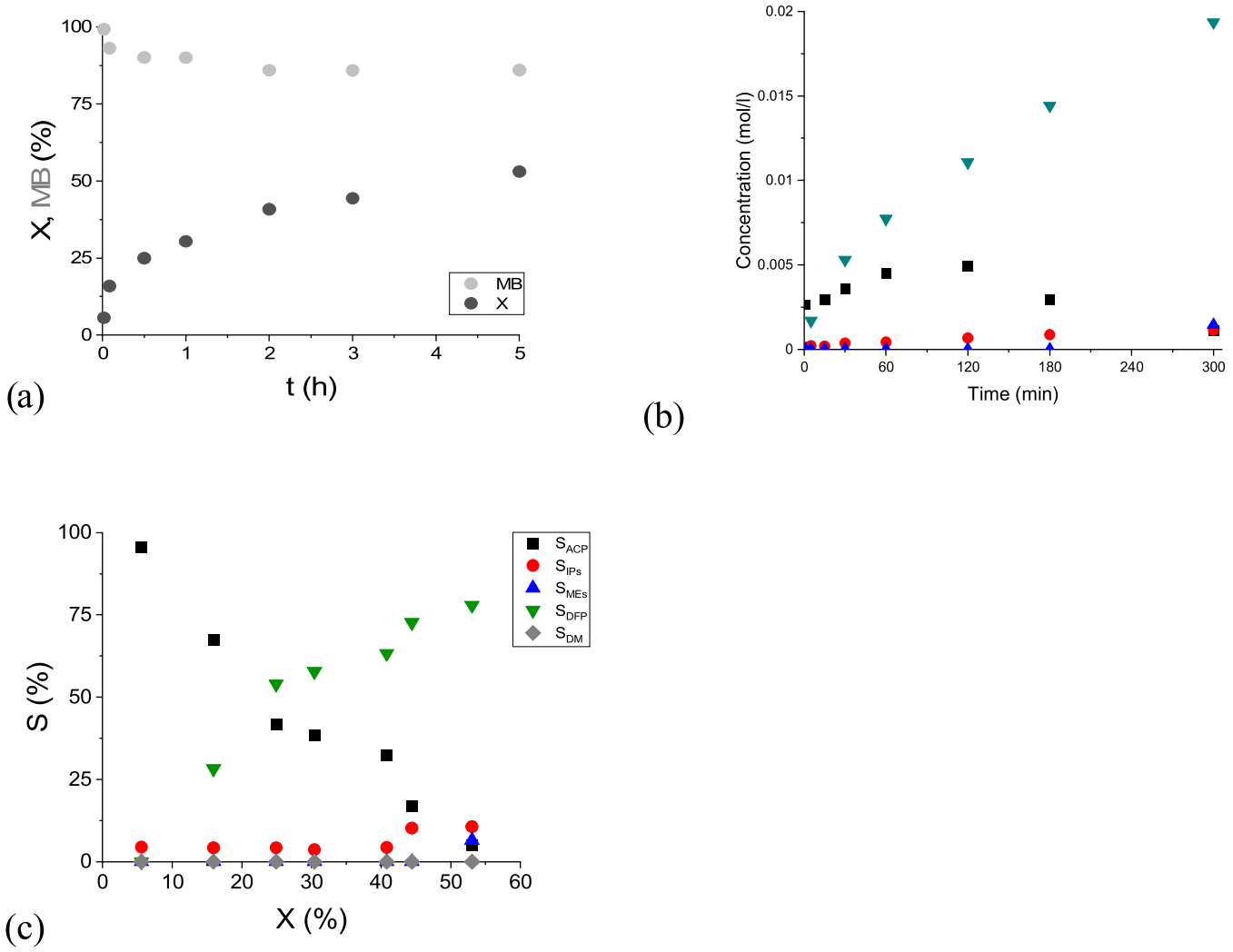

Figure 5. (a) Citral conversion (X) and liquid phase mass balance closure (MB), (b) concentrations of different products in a batch reactor, and (c) selectivity as a function of conversion. Legend: ACP—acyclic hydrogenation products, IPs—isopulegol isomers, MEs—menthol isomers, DFP—defunctionalization products, and DM—dimeric ethers and heavy components. Conditions: 70 °C, 10 bar of H_2, 0.086 M initial concentration of citral in cyclohexane, and 0.2 g of the Ni/MAS catalyst. Notation: (■) ACP, (●) IPs, (▲) MEs, (▼) DFP, and (♦) DM.

Brønsted and Lewis acid sites ratio (B/L), 0.9, were obtained for 5 wt % Ni/MAS. When Ni is loaded in zeolites and mesoporous catalysts, typically, the amount of strong acid Brønsted sites decreases as confirmed by Kubička et al.[31] The same B/L ratio and overall lower values for both Brønsted and Lewis acid sites were obtained for Ni/(MAS + sepiolite) extrudates compared to the powder catalyst without sepiolite binder.

SEM images of fresh powder catalysts, nonreduced (Figure 4a) and reduced (Figure 4b), are in line with the results from nitrogen physisorption (Table 1) and clearly show structural reordering after the reduction procedure (350 °C). The same trend was observed in case of extrudates. The spent extrudates exhibited a more compacted surface, which could be related to additional structural reordering and the blockage of pores after the reaction. The Si/Al weight ratio was 5.15 for both nonreduced and reduced powder catalysts. A slightly higher Si/Al weight ratio of 5.86 was detected for extrudates containing the sepiolite binder, which is consistent with a lower acidity of Ni/(MAS + sepiolite) compared to Ni/MAS detected by FTIR analysis of pyridine adsorption (Table 2).

The mechanical strengths of extrudates were determined to be 32 ± 7 and 4 ± 1 bar in the vertical and horizontal positions, respectively. These are relatively high compared to the mechanical strengths of aluminosilicate extrudates[32] calcined at 600 and 800 °C, i.e., 4.2 and 25 bar, respectively. A higher value for Ni/(MAS + sepiolite) extrudates in the current work can be attributed to the sepiolite binder and the presence of the metal in the extrudates. Pure sepiolite extrudates exhibited mechanical strengths of 56 ± 6 and 35 ± 4 bar in vertical and horizontal positions, respectively.[33] For Pt/H-β-25 extrudates containing SiO_2 Bindzil binder or Bentonite binder, the mechanical strengths were 29−45 and 32−48 bar in the vertical position.[30,34]

Activity and Selectivity of the Powder Ni Catalyst in the Batch Experiment. The catalytic results from a batch experiment with 5 wt % Ni/MAS powder catalyst are displayed in Figure 5a−c. Citral conversion (X) increased with time to 53% in 5 h, while the liquid mass balance closure (MB) slightly decreased to 88%. Previously, Ni on MCM-41[19] was used for one-pot transformations of citral to menthol also in cyclohexane at the same temperature and hydrogen pressure as in the current work. The catalyst-to-substrate ratio was, however, much higher (6-fold), resulting in complete conversion already after 2 h. In addition, it should be pointed out here that Mäki-Arvela et al.[19]

https://doi.org/10.1021/acs.oprd.1c00435
Org. Process Res. Dev. 2022, 26, 387−403

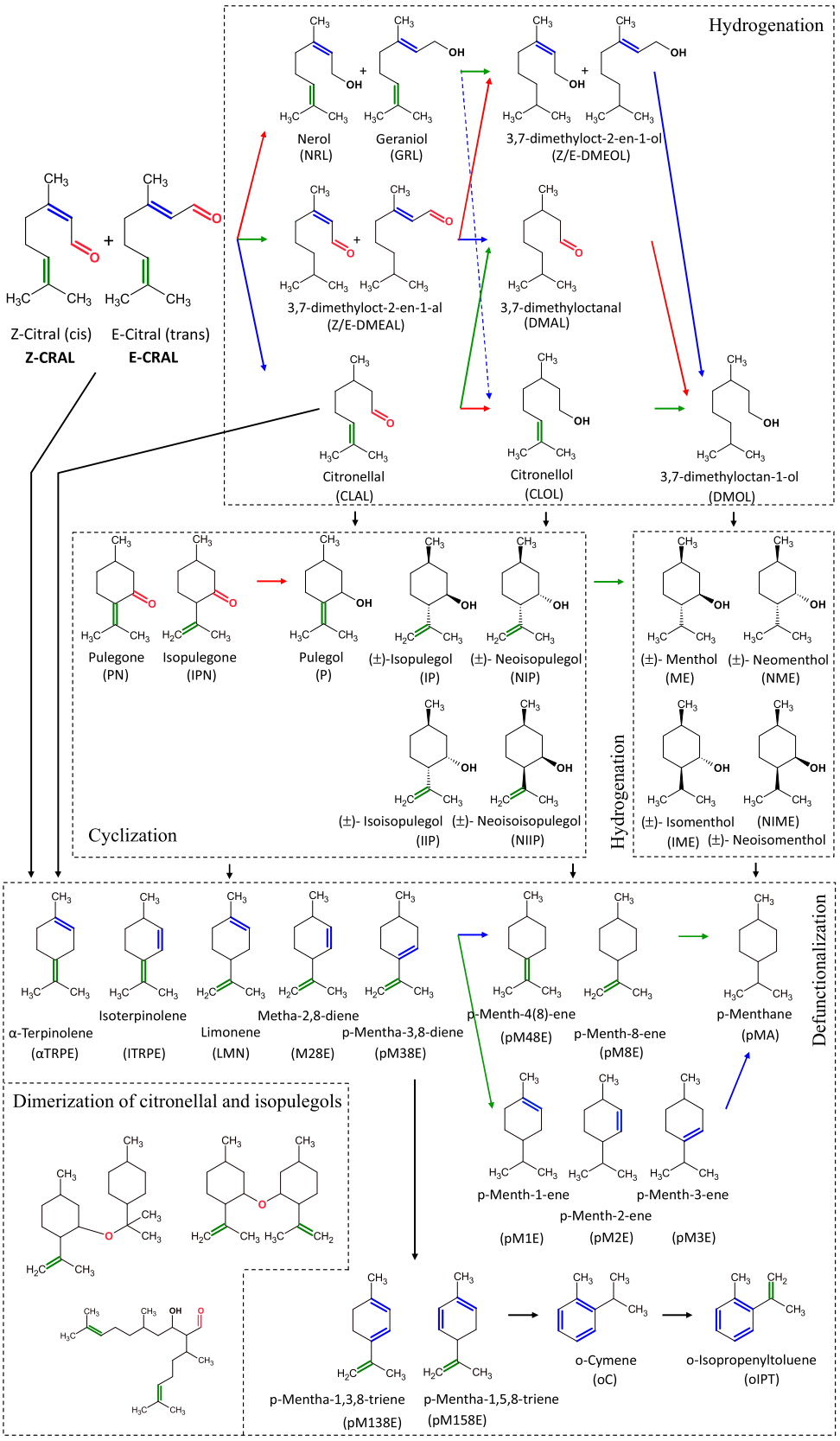

Figure 6. Scheme of menthol synthesis from citral with potential side reactions. Reproduced from Vajglová et al.[20] with permission from the Royal Society of Chemistry. Copyright [2021] [Royal Society of Chemistry].

reported both citral and solvent were preheated and saturated with hydrogen prior to their injection into the reactor, which contained the prereduced catalyst. This pretreatment ensured rapid start up and also faster reaction, while in the current case, prereduced catalyst, reactant, and solvent were loaded into the reactor and the reaction was started when reaching the desired

https://doi.org/10.1021/acs.oprd.1c00435
Org. Process Res. Dev. 2022, 26, 387−403

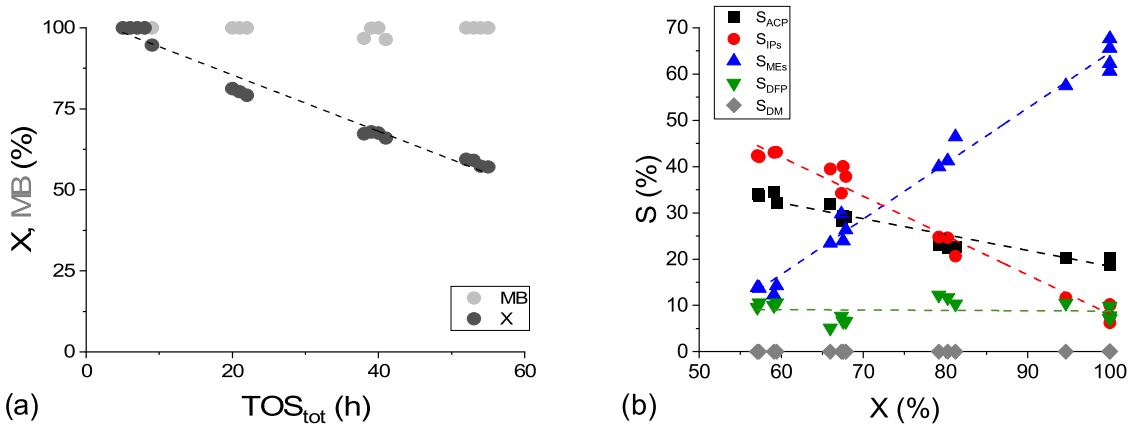

Figure 7. Transformations of citral in a continuous reactor: (a) citral conversion (X) and liquid phase mass balance closure (MB) and (b) selectivity as a function of conversion. Legend: ACP—acyclic hydrogenation products, IPs—isopulegol isomers, MEs—menthol isomers, DFP—defunctionalization products, and DM—dimeric ethers and heavy components. Conditions: 70 °C, 10 bar of H_2, 0.4 mL/min of feed, 0.086 M initial concentration of citral in cyclohexane, 1 g of the Ni/(MAS + sepiolite) catalyst, and 11.5 min of residence time.

temperature and pressure. Although the initial hydrogenolysis rate over 5 wt % Ni-MCM-41 was negligible compared to the initial hydrogenation rate, the selectivity to DFP products after 330 min at 100% conversion was 40%. However, the selectivity to menthols was 54% at the same point and only traces of acyclic hydrogenation products were formed.[19] This catalyst exhibited 5.8 nm Ni particles and the support exhibited a BAS/LAS ratio of 0.53.

In the current work, already during the first minute of the experiment, citral was selectively hydrogenated to citronellal (S = 96%), which was partially converted to isopulegols (S = 4%). The concentration profiles for different product groups, i.e., acyclic hydrogenation products (ACP), pulegols (IPs), menthols (MEs), and defunctionalized products (DFP) are shown in Figure 5b. The scheme of citral transformation demonstrating all potential reactions in detail is shown in Figure 6. The ratio between the initial rates for IPs, ACP, and DFP, i.e., $r_{0,IPs}/r_{0,ACP}/r_{0,DFP}$, is 1:4.6:27.7, while menthols are only visible at 300 min. This result indicates that hydrogenated products were already formed during the heating period as a large amount of citronellal was present at 1 min. Furthermore, a maximum concentration of hydrogenation products was visible at 120 min after which mainly citronellal reacted further to cyclic products. It can also be stated that IPs and MEs were intermediates, which reacted very rapidly to menthenes, while no hydrogenated menthanes were formed. The selectivity to DFP increased with increasing conversion reaching 78% after 5 h (Figure 5c). At the same time, the selectivity to citronellal, which was the only acyclic hydrogenation product, decreased. This result indicates that hydrogenation of citral proceeded during 5 h reaction time; however, its rate decreased because only 53% conversion was achieved. No other hydrogenation products than citronellal were formed over a bifunctional Ni catalyst, which agrees well with data reported by Mäki-Arvela et al.[19] It is worth to note that also a bifunctional Pd/MCM-41 extensively promoted the formation of 3,7-dimethyloctanol.[19] Extensive hydrogenolysis of menthols occurred during 5 h; however, only unsaturated menthene derivatives, i.e., *α*-terpinolene, mentha-2,8-diene, *p*-menth-4(8)-ene, *p*-mentha-1,3,8-triene, *p*-mentha-1,5,8-triene, and *o*-cymene, were formed. The high selectivity to DFP products can be explained by a relatively high BAS/LAS ratio of 0.93 (Table 2) as well as larger Ni particle size, 8 nm, in comparison to ref 19.

Selectivities to isopulegols and menthols after 5 h were only 11 and 6%, respectively (Figure 5c). Stereoselectivity to the desired menthol isomer was 40%. This relatively low value could be attributed to an overall low selectivity to menthols at the citral conversion level achieved after 5 h of the reaction (i.e., 53%). Stereoselectivity to menthol was only 40% after 5 h reaction time in a batch reactor, while in ref 19 it was 70%. This result might also be explained by the slow reaction rate in comparison to ref 19. Typically, (±)-menthol exhibits stereoselectivity in the range of 66−71%.[19,27]

Activity and Selectivity of Ni Extrudates in the Continuous Operation Mode. One-pot citral transformation experiments at 70 °C, 10 bar of hydrogen, and 0.4 mL/min of feed in the trickle-bed reactor over Ni/(MAS+sepiolite) extrudates demonstrated rather high citral conversion and exceptionally high selectivity to menthols of ca. 75% (Figure 7). The yield of menthols of 63% was previously reported over 8 wt % Ni on heteropolyacid with a mesoporous support[17] after 24 h of the reaction at 80 °C and 10 bar of hydrogen. Lower yields (35−50%) were reported for other studied catalysts. The authors[17] concluded that the presence of strong Lewis and medium Brønsted acid sites is required for high menthol selectivity. Note that for the Ru/MCM-41 catalyst[20] also tested in the form of extrudates with the Bindzil binder, mainly defunctionalized products were obtained (ca. 25−30% yield) and the highest yield of menthol was just 6% with a stereoselectivity of 66%. Analogous to the previous work on the ruthenium catalyst in a trickle-bed reactor, substantial catalyst deactivation was seen resulting not only in a decrease of the conversion but also significant selectivity changes with increasing time-on-stream (TOS) as conversion was decreased because of deactivation (Figure 7).

A decrease in the catalytic activity can be caused by Ni leaching as well as by pore blocking (Table 1). The subsequent changes in selectivity are in fact expected for a consecutive reaction network.

The citral conversion and selectivity to the desired menthols (MEs) decreased by 0.9 and 1.1% per hour of TOS, respectively. On the contrary, selectivity to isopulegols (IPs) and the acyclic hydrogenation products (ACP) during the same time increased by 0.7 and 0.3%, respectively. Selectivity to the defunctionalization products (DFP) was constant, not changing with conversion, indicating that such products are formed in parallel

https://doi.org/10.1021/acs.oprd.1c00435
Org. Process Res. Dev. 2022, 26, 387−403

from all reactants and products as illustrated in Figure 6. Neither dimeric ethers nor heavy components (DM) were detected in the reaction mixture. The carbon balance and liquid phase mass balance closure (MB) were close to 100%. Note that much lower mass balance closure was reported for one-pot citral transformations over Ru/MCM-41 containing extrudates finally reaching 60−80% depending on the type of catalyst.[20] Moreover, even the activity decrease was more pronounced in the case of Ru/MCM-41 as conversion dropped from ca. 90−100 to 65−70% just within 3 h.[20]

As expected, detailed analysis of the acyclic hydrogenation products (ACP, Figure 8) revealed an increased selectivity to

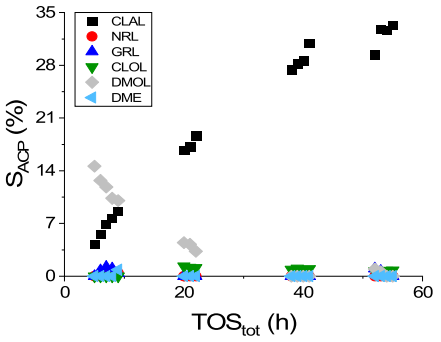

Figure 8. Selectivity to acyclic hydrogenation products as a function of total time-on-stream in a continuous reactor. Legend: CLAL—citronellal, NRL—nerol, GRL—geraniol, CLOL—citronellol, DMOL—3,7-dimethyloctan-1-ol, and DME—2,6-dimethyloctane. Conditions: 70 °C, 10 bar of H_2, 0.4 mL/min of feed, 0.086 M initial concentration of citral in cyclohexane, 1 g of the Ni/(MAS + sepiolite) catalyst, and 11.5 min of residence time.

citronellal, formed in the first step from citral, with TOS at the expense of the subsequent hydrogenation product 3,7-dimethyloctan-1-ol. Other ACP (including 2,6-dimethyloctane) were formed in minor quantities without a visible trend in TOS.

Stereoselectivity to isopulegol and menthol isomers as a function of time-on-stream is displayed in Figures 9 and 10.

In both cases, stereoselectivity only slightly changed with conversion and TOS. Among cyclization products, selectivity to isopulegol and isoisopulegol increased, while selectivity to neoisopulegol clearly decreased with TOS. In 50 h of TOS, the ratio of isopulegol/neoisopulegol/isoisopulegol/neoisopulegol changed from 54/46/0/0 to 61/32/7/0. Often, the distribution of isopulegols follows the thermodynamic equilibrium,[35,36] which means that stereoselectivity to (±)-isopulegol is ca. 70−75%. At the same time, stereoselectivity to isopulegol depends on acidity and over such Lewis acids as Zr-β or zinc chloride, it can reach 90−94% in citronellal cyclization.[35,37] Lower values than thermodynamic ones have also been reported; thus, the stereoselectivity distribution of ca. 55/ 35/10% for IP/ NIP/ IIP was observed for ruthenium bearing extrudates with a random Ru deposition on both H-MCM-41 and Bindzil in one-pot citral transformations to menthol.[20]

Changes in the stereoselectivity distribution of isopulegols were concomitant with the ratio of menthols; thus, the formation of menthol and neomenthol followed selectivity patterns for isopulegol and neoisopulegol. For menthol/neomenthol/isomenthol/neoisomenthol, their ratio changed from 66/26/2/6 to 71/15/0/14 in 50 h of TOS.

Stereoselectivity to the desired (±)-menthol of 68−70% was reported previously for Ru/H-MCM-41 extrudates containing the Bindzil binder,[20] while somewhat lower stereoselectivity to menthol (42%) was obtained for Ru/Y-80 extrudates when Bindzil was used as a binder.[23] Note that the total yield of menthols in previous reports[20,23] for continuous one-pot transformations of citral was much lower (just between 2 and 6%) than in the current work.

Figure 11 shows citral conversion as a function of time-on-stream at different temperatures (40−80 °C) and the same pressure of hydrogen (10 bar), flowrate of feed (0.4 mL/min), and initial citral concentration in cyclohexane (0.086 M) over 1 g of Ni-containing extrudates.

Figure 11 also demonstrates catalyst deactivation visible through a decrease of the conversion with time-on-stream at isothermal conditions as well as by the difference in the level of conversion when the same temperature was tested after several hours of operation.

Figure 12 displaying citral conversion as a function of time-on-stream at different hydrogen pressures (2.5−10 bar) and the same temperature (70 °C) shows almost zero-order dependence in hydrogen for hydrogenation of citral. Somewhat more prominent deactivation was observed at a lower hydrogen pressure that could be probably related to slower recovery of metallic nickel at a lower H_2 pressure.

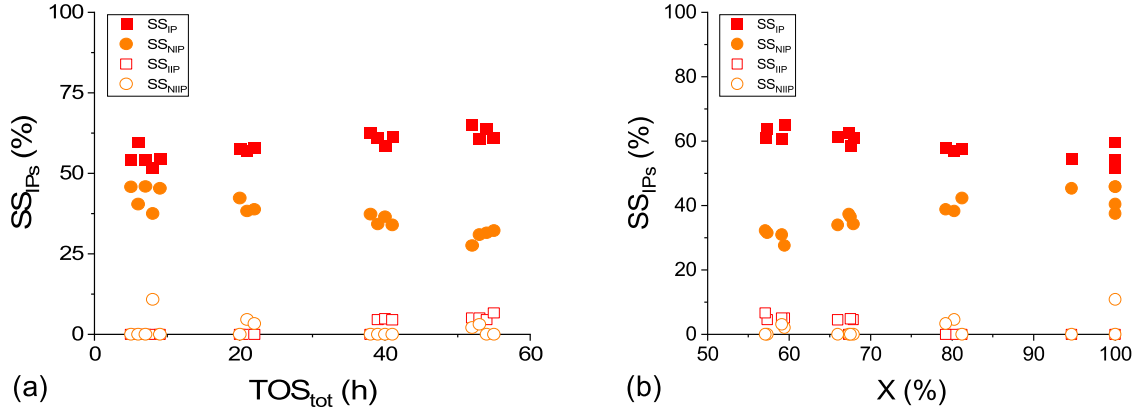

Figure 9. Stereoselectivity to isopulegol isomers (SS_{IPs}) in a continuous reactor as a function of (a) total time-on-stream and (b) conversion. Legend: IP—isopulegol, NIP—neoisopulegol, IIP—isoisopulegol, and NIIP—neoisoisopulegol. Conditions: 70 °C, 10 bar of H_2, 0.4 mL/min of feed, 0.086 M initial concentration of citral in cyclohexane, 1 g of the Ni/(MAS + sepiolite) catalyst, and 11.5 min of residence time.

https://doi.org/10.1021/acs.oprd.1c00435
Org. Process Res. Dev. 2022, 26, 387−403

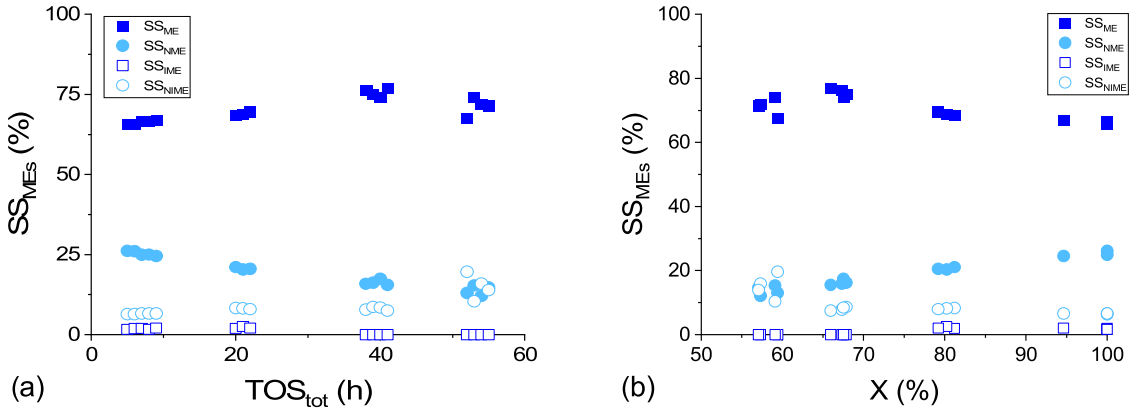

Figure 10. Stereoselectivity to menthol isomers (SS_{MEs}) in a continuous reactor as a function of (a) total time-on-stream and (b) conversion (X). Legend: ME—menthol, NME—neomenthol, IME—isomenthol, and NIME—neoisomenthol. Conditions: 70 °C, 10 bar of H_2, 0.4 mL/min of feed, 0.086 M initial concentration of citral in cyclohexane, 1 g of the Ni/(MAS + sepiolite) catalyst, and 11.5 min of residence time.

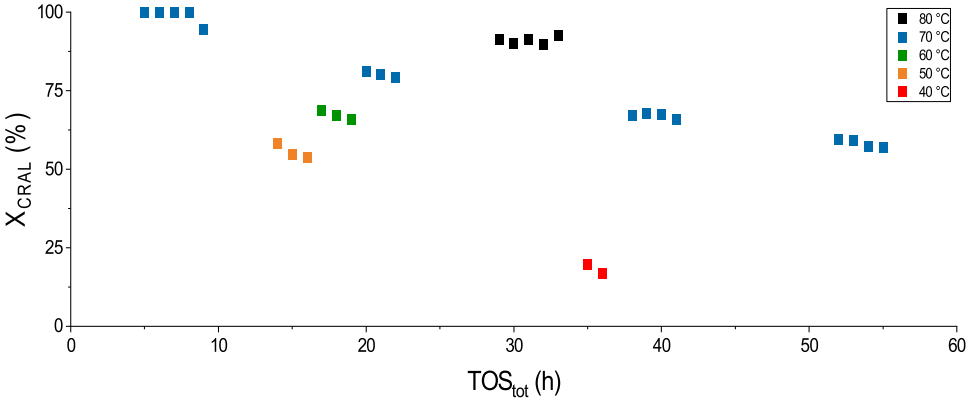

Figure 11. Citral conversion as a function of total time-on-stream at different temperatures in a continuous reactor. Conditions: 40−80 °C, 10 bar of H_2, 0.4 mL/min of feed, 0.086 M initial concentration of citral in cyclohexane, 1 g of the Ni/(MAS + sepiolite) catalyst, and 11.5 min of residence time.

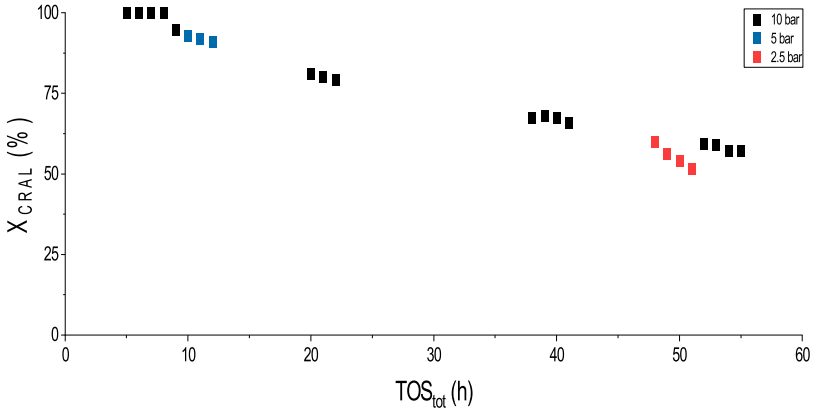

Figure 12. Citral conversion as a function of total time-on-stream at different pressures in a continuous reactor. Conditions: 70 °C, 2.5−10 bar of H_2, 0.4 mL/min of feed, 0.086 M initial concentration of citral in cyclohexane, 1 g of the Ni/(MAS+sepiolite) catalyst, and 11.5 min of residence time.

KINETIC MODELING

Kinetic analysis of one-pot transformations of citronellal to menthols in a batch reactor has been reported for the Ru/β-25 catalyst,[37] while such analysis is absent for citral transformations to menthol for both batch and continuous operation modes.

In the current work, we have thus developed a kinetic model capable of describing experimental data for transformations of citral to menthol in a continuous mode.

The reaction network is an extension of the network proposed previously for one-pot transformations of citronellal to menthol[38] and includes hydrogenation of citral to citronellal and side transformations to defunctionalized products (Figure 13).

The noncompetitive adsorption of organic compounds and hydrogen allows the introduction of the rate expressions for the following type

$$r_1 = \frac{k_1 c_{\text{Citral}} P}{D\, D_{H_2}} \alpha_1 \rho_B \qquad (1)$$

https://doi.org/10.1021/acs.oprd.1c00435
Org. Process Res. Dev. 2022, 26, 387−403

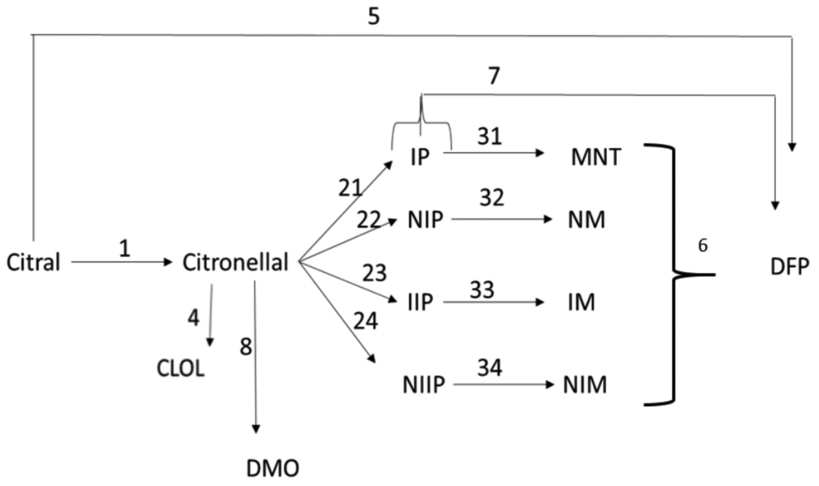

Figure 13. Reaction network for one-pot transformations of citral to menthol. Legend: IP—isopulegol, NIP—neoisopulegol, IIP—isoisopulegol, NIIP—neoisoisopulegol, MNT—menthol, NM—neomenthol, IM—isomenthol, NIM—neoisomenthol, DMO—dimethyloctanol, DFP—defunctionalized products, and CLOL—cintronellol.

where k_1 is the lumped rate constant, which includes adsorption constants of hydrogen and citral, P is the hydrogen pressure, ρ_B is the catalyst bulk density (0.217 g/cm^3), r_1 is the reaction rate along path 1, c_{citral} is the concentration of citral (mol/L), and D and D_{H2} are denominators

$$D = 1 + K_A\, c_{Citral} + K_B c_{Citronellal} + K_C(c_{IP} + c_{NIP} + c_{IIP} + c_{NIIP}) + K_D(c_{MNT} + c_{NM} + c_{IM} + c_{NIM}) + K_F c_{DFP} \quad (2)$$

$$D_{H_2} = 1 + K_{H_2} P \quad (3)$$

In eqs 2 and 3, K_A, K_B, K_C, K_D, K_F, and K_{H_2} are equilibrium constants for adsorption of citral, citronellal, isopulegols, menthols, defunctionalized products, and hydrogen, respectively.

The term α_1 reflects catalyst deactivation, which was modeled in a semiempirical way[24,39,40] by introducing an exponential decay function of metal sites with TOS

$$\alpha_1 = e^{-k_{d1}\,TOS} \quad (4)$$

where k_{d1} is the temperature-dependent deactivation constant.

For the cyclization reaction routes (reactions 21−24), the expressions for the observed rates can be written as follows

$$r_{2,1-4} = \eta_{2,1-4} \frac{k_{2,1-4} c_{Citronellal}}{D} \alpha_2 \rho_B \quad (5)$$

With another deactivation function, specific for acidic sites

$$\alpha_2 = e^{-k_{d2}\,TOS} \quad (6)$$

where k_{d2} is the temperature-dependent deactivation constant for acidic sites. During the parameter estimation, it turned out, however, that the temperature dependence of this and the first deactivation constant could be neglected. In eq 5, η is the catalyst effectiveness factor for a particular reaction reflecting the experimental data in this work were generated in the regime where the external and internal mass transfer cannot be neglected. In general, for nonfirst-order reactions, the catalyst effectiveness factor changes during the reaction as the Thiele modulus depends on the concentration.

In the current work for hydrogenation reactions of isopulegols to menthols on metallic sites, the rate expressions are

$$r_{31} = \eta_{31} \frac{k_{31} c_{IP}\, P}{D\, D_{H_2}} \alpha_1 \rho_B;\; r_{32} = \eta_{32} \frac{k_{32} c_{NIP} P}{D\, D_{H_2}} \alpha_1 \rho_B;\; r_{33} = \eta_{33} \frac{k_{33} c_{IIP}\, P}{D\, D_{H_2}} \alpha_1 \rho_B; r_{34} = \eta_{34} \frac{k_{34} c_{NIIP} P}{D\, D_{H_2}} \alpha_1 \rho_B \quad (7)$$

The initial kinetic model included step 4; however, because the yields of citronellol were very low, this step was excluded from further considerations. Moreover, numerical data fitting indicated that because of lumping of defunctionalized products into one group, it is sufficient to include only the rate of reaction 5 in the model, finally giving

$$r_5 = \eta_5 \frac{k_5(c_{Citral})}{D} \alpha_1\, \rho_B \quad (8)$$

$$r_7 = \eta_7 \frac{k_7(c_{IP} + c_{NIP} + c_{IIP} + c_{NIIP})P}{D\, D_{H_2}} \alpha_1 \rho_B \quad (9)$$

$$r_8 = \eta_8 \frac{k_8 c_{Citronellal} P}{D\, D_{H_2}} \alpha_1 \rho_B \quad (10)$$

The plug flow reactor model was used, solving the rate equations along with mass balances

$$\frac{dc_{Citral}}{d_\tau} = -r_1 - r_5;\; \frac{dc_{Citronellal}}{d_\tau} = r_1 - r_{21} - r_{22} - r_{23} - r_{24} - r_8$$

$$\frac{dc_{IP}}{d} = r_{21} - r_{31} - r_7 \frac{c_{IP}}{(c_{IP} + c_{NIP} + c_{IIP} + c_{NIIP})};\; \frac{dc_{NIP}}{d} = r_{22} - r_{32} - r_7 \frac{c_{NIP}}{(c_{IP} + c_{NIP} + c_{IIP} + c_{NIIP})}$$

$$\frac{dc_{IIP}}{d} = r_{23} - r_{33} - r_7 \frac{c_{IIP}}{(c_{IP} + c_{NIP} + c_{IIP} + c_{NIIP})};\; \frac{dc_{NIIP}}{d} = r_{24} - r_{34} - r_7 \frac{c_{NIIP}}{(c_{IP} + c_{NIP} + c_{IIP} + c_{NIIP})}$$

https://doi.org/10.1021/acs.oprd.1c00435
Org. Process Res. Dev. 2022, 26, 387−403

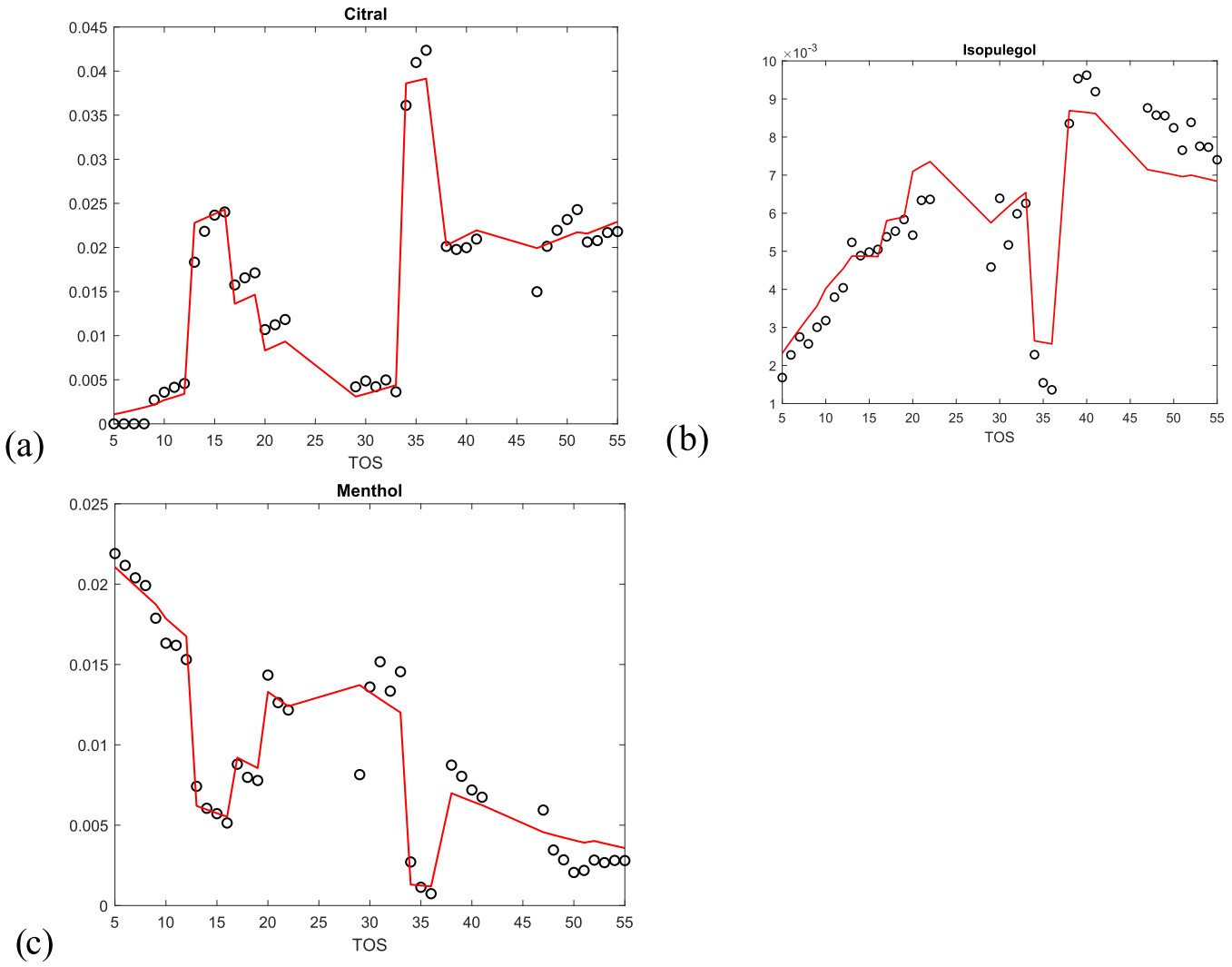

Figure 14. Comparison between experimental and calculated data. Time-on-stream (TOS, h) dependence of (a) citral, (b) isopulegol isomers, and (c) menthol isomers concentrations in mol/L.

$$\frac{dc_{MNT}}{d} = r_{31};\ \frac{dc_{NM}}{dt} = r_{32};\ \frac{dc_{IM}}{dt};\ \frac{dc_{NIM}}{dt} = r_{34};\ \frac{dc_{DMO}}{dt} = r_8\frac{dc_{DFP}}{dt} = r_7 + r_5 \tag{11}$$

where τ is the residence time in min. For the sake of simplicity, the rate constants for transformations of different isomers of isopulegols to defunctionalized products were considered to be equal to each other; thus, the rates of step 7 in eq 11 contain the term corresponding to the fraction of a particular isomer.

During the parameter estimation, average values of the catalyst effectiveness factors for different rates were calculated neglecting their concentration dependencies, as a rather close to first-order kinetic curve could be deduced from the batch data (Figure 5).

The temperature dependence was modeled with the modified Arrhenius equation, where $\overline{T}$ is the mean temperature used in the experiments (i.e., 70 °C)

$$k_j = k_{0j}e^{-\frac{E_{a,j}}{R}\left(\frac{1}{T}-\frac{1}{T_{mean}}\right)} \tag{12}$$

Kinetic modeling was performed using ModEst software,[41] minimizing the residual sum of squares between the calculated and experimental data with the Levenberg−Marquardt and simplex algorithms implemented in the software. The degree of explanation reflecting a comparison between the residuals given by the model with the residuals of the simplest model, i.e., the average value of all data points,[40] served as a measure of the fit quality.

Application of eq 11 along with the expressions for the rates for various steps in the reaction mechanism (eqs 1,5, 7−10) gave a reliable description of experimental data (Figures 14 and S4) with the degree of explanation equal to 97.1%. The values of parameters are presented in Table 3.

In general, the parameters are rather well-identified apart from E_{a34} and activation energy for deactivation steps, exhibiting a very minor temperature dependence. Due to a large number of parameters, errors for some constants were in the range of 50% and a certain correlation between them was seen. Figure 15 illustrates examples of such correlations.

Elongated contour plots visible in some of the graphs in Figure 15 reflect a strong correlation between some parameters. It should be, however, considered that this study represents a first example of successful one-pot transformation of citral to menthol in a continuous reactor over a supported nickel catalyst shaped to extrudates along with a binder and apparently more

https://doi.org/10.1021/acs.oprd.1c00435
Org. Process Res. Dev. 2022, 26, 387−403

Table 3. Values of Kinetic Parameters

constant	value	error (%)	units
$\eta_1 k_1$	52.9	56.8	mol/(g bar min)
$\eta_{21} k_{21}$	8.11	45.6	mol/(g min)
$\eta_{22} k_{22}$	3.54	45.5	mol/(g min)
$\eta_{24} k_{24}$	1.18	51.3	mol/(g min)
$\eta_{31} k_{31}$	77.6	56.8	mol/(g bar min)
$\eta_{32} k_{32}$	45.0	56.4	mol/(g bar min)
$\eta_{34} k_{34}$	40.2	57.6	mol/(g bar min)
$\eta_5 \mathbf{k}_5$	4.7	59.2	mol/(g bar min)
$\eta_7 k_7$	4.07	60.0	mol/(g bar min)
$\eta_8 k_8$	7.1	56.3	mol/(g bar min)
E_{a1}	80.7	4.7	kJ/mol
E_{a21}	38.1	10.4	kJ/mol
E_{a22}	37.9	13.0	kJ/mol
E_{a24}	92.2	18.7	kJ/mol
E_{a31}	45.5	7.9	kJ/mol
E_{a32}	48.8	13.3	kJ/mol
E_{a34}	not reliable	not reliable	kJ/mol
E_{a5}	56.8	11.5	kJ/mol
E_{a7}	111	20.2	kJ/mol
E_{a8}	40.7	20.7	kJ/mol
K_C	749	52.3	L/mol
K_H	4.5	41.6	1/bar
k_{d1}	0.037	2.8	l/min
k_{d2}	0.0175	8.8	l/min

work is needed to determine the values of kinetic parameters in a more statistically reliable way.

CONCLUSIONS

A 5% Ni on mesoporous aluminosilicate and sepiolite (as a binder) catalyst was prepared by extrusion and tested in one-pot menthol synthesis from citral at 40−80 °C under varied hydrogen pressures between 2.5 and 10.0 bar. After deposition of nickel, the mesoporous structure of the support was preserved in the catalyst, which exhibited the size of metal clusters of ca. 10 nm.

The time-on-stream conversion of citral, which was initially complete, decreased to ca. 60%. Simultaneously high selectivity to menthols (above 70%), substantially exceeding previously reported values for one-pot transformations with citral as the reactant in a continuous reactor, decreased because of lower conversion. In addition to the main product and the reaction intermediates, the defunctionalized products were also formed with ca. 10% overall selectivity. Selectivity to these products was constant with conversion as a result of parallel pathways of their generation from all reactants and products.

Stereoselectivity to menthols and isopulegols only slightly changed with conversion and time-on-stream (TOS) being in the range of 66−71% for the desired (±)-menthol.

Citral conversion as a function of time-on-stream was almost independent of hydrogen pressure at 70 °C with somewhat more prominent deactivation at a lower hydrogen pressure.

Kinetic analysis for citral transformations to menthol for both batch and continuous operation modes is absent in the open literature; thus, in the current work, a kinetic model capable of describing experimental data for transformations of citral to menthol in a continuous mode was developed for the first time. The model, including formation of the main reaction as well as side products, takes into account catalyst deactivation on two types of sites of the bifunctional catalyst. Numerical data fitting performed for the whole experimental data set confirmed applicability of the advanced kinetic model.

EXPERIMENTAL SECTION

Preparation of the Ni Catalyst. Mesoporous aluminosilicate (MAS) as a support and sepiolite ($Mg_2H_2SiO_9\ xH_2O$, Sigma-Aldrich) as a binder were dried overnight at 100 °C and physically mixed in the mass ratio = 70/30, e.g., 4.2 g and 1.8 g, respectively. Methylcellulose (1.0 wt %, e.g., 0.06 g) as an organic binder (viscosity: 4000 cP, Sigma-Aldrich) was dissolved in 3 mL of water and added into the mixture of MAS and sepiolite to control the rheological properties of the final slurry. Distilled water was slowly dropped into the mixture under stirring at room temperature. The extrudates were fabricated in a cylindrical shape with a diameter of 1.4 mm using the extruder equipped with a 1.5-mm diameter-hole die plate (TBL-2, Tianjin Tianda Beiyang Chemical Co. Ltd., China) driven by a rotational velocity of 1400 rpm. Subsequently, the extrudates were dried in an oven at 100 °C overnight, calcined at 500 °C for 4 h in a muffle oven, and cut to a length of ca. 0.6−1.0 cm.

Ni-containing extrudates were prepared by an incipient wetness impregnation with nickel nitrate aqueous solution $Ni(NO_3)_2{\cdot}6H_2O$ (Sigma-Aldrich, >97%) to achieve the nominal nickel loading 5.7 wt %, dried overnight at 100 °C and calcined at 450 °C for 6 h in a muffle oven. Before catalytic run, the synthesized Ni/(MAS+Sepiolite) extrudates were reduced in the reactor in hydrogen flow (100 mL/min) at 350 °C during 2.5 h with a temperature ramp of 2 °C/min.

The 5 wt % Ni/MAS powder catalyst was prepared by the incipient wetness impregnation with an aqueous solution of $Ni(NO_3)_2{\cdot}6H_2O$ (CJSC Souzchimprom). Thereafter, the sample was dried at 100 °C overnight and calcined at 450 °C for 6 h with a temperature ramp of 2 °C/min controlling decomposition of nickel nitrate by measuring the pH of the outgoing gases. Before a catalytic run, calcined Ni/MAS powder catalysts were activated in hydrogen flow at 350 °C during 2 h with the temperature ramp of 2 °C/min.

Characterization of Ni Catalysts. Fresh and spent Ni catalysts in the powder and shaped forms were characterized in detail. Inductively coupled plasma-optical emission spectrometry determined the metal concentration in the entire volume of the catalyst with the PerkinElmer Optima 5300 DV device.

Transmission electron microscopy using JEOL JEM-1400Plus was used to investigate the metal shape, particle size, and metal location.

Morphological studies were performed by scanning electron microscopy (SEM, Zeiss Leo Gemini 1530). Elemental analysis of microporous materials was conducted by energy-dispersive X-ray microanalysis using the same instrument.

Nitrogen physisorption was used to determine the pore size distribution, pore volume, and specific surface area with the Micromeritics 3Flex-3500 machine.

Fourier transform infrared spectroscopy with pyridine as a probe molecule was applied to quantify the amount and strength of Brønsted and Lewis acid sites using an ATI Mattson FTIR Infinity series spectrometer.

Powder X-ray diffraction (XRD) patterns of extrudates were obtained on a Bruker D8 Advance diffractometer (Cu Kα radiation, λ = 0.15418 nm) equipped with a LynxEye position-sensitive detector. The data were collected in the 2θ range of 5−65° with a step of 0.05° and a collection time of 3 s. Phase identification was performed using the ICDD PDF-2 database

https://doi.org/10.1021/acs.oprd.1c00435
Org. Process Res. Dev. 2022, 26, 387−403

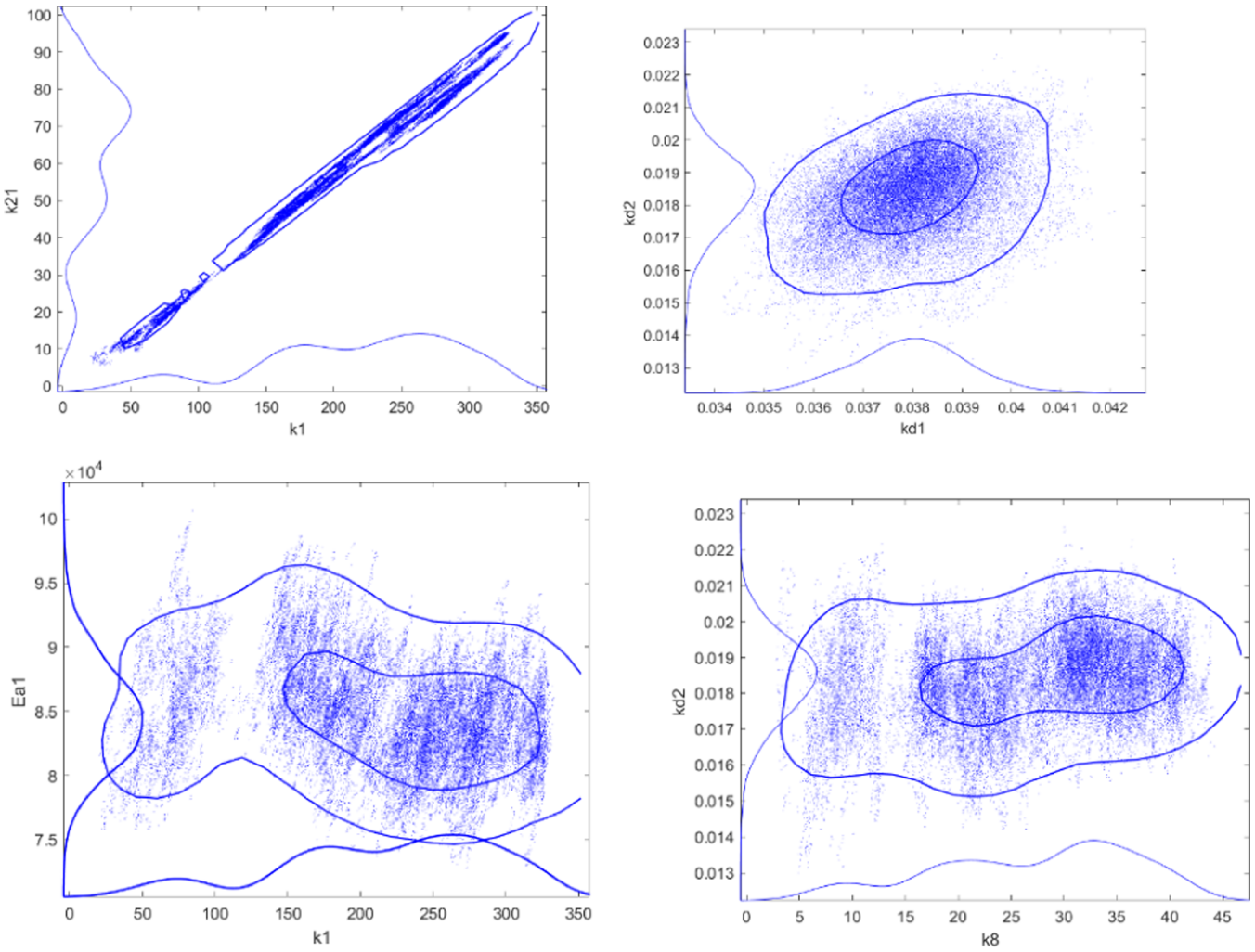

Figure 15. Examples of correlations between kinetic parameters. The units of parameters are shown in Table 3.

[Powder Diffraction File database PDF-2, International Centre for Diffraction Data, 2009]. The average crystallite size of phases was calculated by the line broadening analysis according to the Scherrer equation.

The mechanical strength of the shaped catalyst was measured by the crush tester (SE 048, Lorentzen & Wettre) for 10 extrudates in the vertical position and 10 extrudates in the horizontal position.

Details of characterization methods and instruments are reported in our previous publications.[20,25,26,30,42−44]

Catalytic Tests. The experiments of citral transformations over Ni/(MAS + Sepiolite) extrudates were carried out in a continuous trickle-bed reactor (internal diameter 1.25 cm, empty reactor volume 14.7 mL, catalyst bed volume 4.6 mL)[20,23,25−27] at different temperatures 40, 50, 60, 70, and 80 °C under varied hydrogen pressures of 2.5, 5.0, and 10.0 bar. A quartz wool was placed at the bottom of the reactor, then 1 g of Ni/(MAS + Sepiolite) extrudates as well as inert quartz beads of the size in the range 0.2−0.8 mm (~18 g) were loaded inside the reactor, filling the voids between extrudates and in the reactor. Citral (cis-/trans-isomer ~1/1, ≥95.0%, Sigma-Aldrich) in cyclohexane (≥99.9%, Alfa Aesar) solution (0.086 M) was fed into the reactor with a feeding rate of 0.4 mL/min, while the hydrogen rate was 100 mL/min.

A 5 wt % Ni/MAS powder catalyst was tested in the autoclave (Parr, 300 mL). The experiment was performed over 0.2 g of the catalyst at 70 °C, 10 bar of H_2 with 0.086 M citral in cyclohexane, and 900 rpm.

The liquid samples were analyzed by gas chromatography with flame-ionization detection using Agilent GC 6890 N. All samples were diluted with cyclohexane as a solvent before analysis. The column was DB-1 column with a length of 30 m, diameter of 250 μm, and film thickness of 0.5 μm. Temperature program: 110 °C−0.4 °C/min−130 °C−13 °C/min−200 °C (5 min). Details are given in our previous publications.[20,23,25−27]

■ ASSOCIATED CONTENT

Supporting Information

The Supporting Information is available free of charge at https://pubs.acs.org/doi/10.1021/acs.oprd.1c00435.

Isotherms of adsorption/desorption (powdered and extruded catalysts), pore size distribution (powdered and extruded catalysts), parity plots for all reaction components, and XRD patterns of powdered Ni/MAS catalysts (PDF)

https://doi.org/10.1021/acs.oprd.1c00435
Org. Process Res. Dev. 2022, 26, 387−403

AUTHOR INFORMATION

Corresponding Author

Dmitry Yu. Murzin − *Johan Gadolin Process Chemistry Centre, Åbo Akademi University, Turku/Åbo 20500, Finland;* orcid.org/0000-0003-0788-2643; Email: dmurzin@abo.fi

Authors

Irina L. Simakova − *Boreskov Institute of Catalysis, 630090 Novosibirsk, Russia;* orcid.org/0000-0002-5138-4847

Zuzana Vajglová − *Johan Gadolin Process Chemistry Centre, Åbo Akademi University, Turku/Åbo 20500, Finland*

Päivi Mäki-Arvela − *Johan Gadolin Process Chemistry Centre, Åbo Akademi University, Turku/Åbo 20500, Finland;* orcid.org/0000-0002-7055-9358

Kari Eränen − *Johan Gadolin Process Chemistry Centre, Åbo Akademi University, Turku/Åbo 20500, Finland*

Leena Hupa − *Johan Gadolin Process Chemistry Centre, Åbo Akademi University, Turku/Åbo 20500, Finland*

Markus Peurla − *University of Turku, FI-20520 Turku, Finland*

Ermei M. Mäkilä − *University of Turku, FI-20520 Turku, Finland;* orcid.org/0000-0002-8300-6533

Johan Wärnå − *Johan Gadolin Process Chemistry Centre, Åbo Akademi University, Turku/Åbo 20500, Finland*

Complete contact information is available at: https://pubs.acs.org/10.1021/acs.oprd.1c00435

Notes

The authors declare no competing financial interest.

ACKNOWLEDGMENTS

The authors are grateful to the Academy of Finland for funding through the project: Synthesis of spatially controlled catalysts with superior performance. Electron microscopy samples were processed and analyzed at the Electron Microscopy Laboratory, Institute of Biomedicine, University of Turku, which receives financial support from Biocenter Finland. I.L.S. is grateful for the support from the Ministry of Science and Higher Education of the Russian Federation, under the governmental order for Boreskov Institute of Catalysis (Project No. AAAA-A21-121011390055-8).

REFERENCES

(1) Noyori, R. Asymmetric Catalysis: Science and Opportunities (Nobel Lecture 2001). *Adv. Synth Catal.* **2003**, *345*, 15−32.

(2) Otsuka, S.; Tani, K.; Yamagata, T.; Akutagawa, S.; Kumobayashi, H.; Yagi, M. Process for the preparation of enamines or imines. EP0068506A11983.

(3) Fleischer, J.; Bauer, K.; Hopp, R. Resolution of menthol, neomenthol or isomenthol racemic mixtures by esterification with benzoic acid derivatives. DE2109456A11972.

(4) Besson, M.; Bullivant, L.; Nicolaus, N.; Gallezot, P. Stereoselective Thymol Hydrogenation: I. Kinetics of Thymol Hydrogenation on Charcoal-Supported Platinum Catalysts. *J. Catal.* **1993**, *140*, 30−40.

(5) Allakhverdiev, A. I.; Kul'kova, N. V.; Murzin, D.Yu. Liquid-Phase Stereoselective Thymol Hydrogenation over Supported Nickel Catalysts. *Catal. Lett.* **1994**, *29*, 57−67.

(6) Allakhverdiev, A. I.; Kul'kova, N. V.; Murzin, D.Yu. Kinetics of Thymol Hydrogenation over a Ni-Cr_2O_3 Catalyst. *Ind. Eng. Chem. Res.* **1995**, *34*, 1539−1547.

(7) Cardena, G.; Oliva, R.; Reyes, P. Catalytic Hydrogenation of Thymol over Pd/MgO Prepared by SMAD Method. *J. Chil. Chem. Soc.* **2006**, *51*, 1053−1056.

(8) Dudas, J.; Hanika, J.; Lepuru, J.; Barkhuysen, M. Thymol Hydrogenaton in a Bench Scale Trickle Bed Reactor. *Chem. Biochem. Eng. Quart.* **2005**, *19*, 255−262.

(9) Aumo, J.; Oksanen, S.; Mikkola, J.-P.; Salmi, T.; Murzin, D. Yu. Hydrogenation of Citral over Activated Carbon Cloth Catalyst. *Ind. Eng. Chem. Res.* **2005**, *44*, 5285−5290.

(10) Mäki-Arvela, P.; Tiainen, L.-P.; Lindblad, M.; Demirkan, K.; Kumar, N.; Sjöholm, R.; Ollonqvist, T.; Väyrynen, J.; Salmi, T.; Murzin, D. Yu. Liquid-Phase Hydrogenation of Citral for Production of Citronellol: Catalyst Selection. *Appl. Catal., A* **2003**, *241*, 271−288.

(11) Mäki-Arvela, P.; Kumar, N.; Nieminen, V.; Sjoholm, R.; Salmi, T.; Murzin, D. Yu. Cyclization of Citronellal over Zeolites and Mesoporous Materials for Production of Isopulegol. *J. Catal.* **2004**, *225*, 155−169.

(12) Chuah, G. K.; Liu, S. H.; Jaenicke, S.; Harrison, L. J. Cyclisation of Citronellal to Isopulegol Catalysed by Hydrous Zirconia and Other Solid Acids. *J. Catal.* **2001**, *200*, 352−359.

(13) Gralla, G.; Heydrich, G.; Bergner, E. J.; Ebel, K. Process for preparation of menthol by hydrogenation of isopulegol. U.S. Patent US2010191021A12010.

(14) Nie, Y. T.; Jaenicke, S.; Chuah, G. K. Zr-Zeolite Beta: A New Heterogeneous Catalyst System for the Highly Selective Cascade Transformation of Citral to (+/-)-Menthol. *Chem. Eur. J.* **2009**, *15*, 1991−1999.

(15) Negoi, A.; Teinz, K.; Kemnitz, E.; Wuttke, S.; Parvulescu, V. I.; Coman, S. M. Bifunctional Nanoscopic Catalysts for the One-Pot Synthesis of (+/-)-Menthol from Citral. *Top Catal.* **2012**, *55*, 680−687.

(16) Trasarti, A. F.; Marchi, A. J.; Apesteguia, C. R. Design of Catalyst Systems for the One-Pot Synthesis of Menthols from Citral. *J. Catal.* **2007**, *247*, 155−165.

(17) Shah, A. K.; Maitlo, G.; Shah, A. A.; Channa, I. A.; Kandhro, G. A.; Maitlo, H. A.; Bhatti, U. H.; Shah, A.; Memon, A. Q.; Jatoi, A. S.; Park, Y. H. One Pot Menthol Synthesis via Hydrogenations of Citral and Citronellal over Montmorillonite-Supported Pd/Ni-Heteropoly Acid Bifunctional Catalysts. *React. Kinet., Mech. Catal.* **2019**, *128*, 917−934.

(18) Virtanen, P.; Salmi, T. O.; Mikkola, J. P. Supported Ionic Liquid Catalysts (SILCA) for Preparation of Organic Chemicals. *Top Catal.* **2010**, *53*, 1096−1103.

(19) Mäki-Arvela, P.; Kumar, N.; Kubicka, D.; Nasir, A.; Heikkilä, T.; Lehto, V.-P.; Sjöholm, R.; Salmi, T.; Murzin, D. Yu. One-pot Citral Transformation to Menthol over Bifunctional Micro- and Mesoporous Metal Modified Catalysts: Effect of Catalyst Support and Metal. *J. Mol. Catal. A. Chem.* **2005**, *240*, 72−81.

(20) Vajglová, Z.; Mäki-Arvela, P.; Eränen, K.; Kumar, N.; Peurla, M.; Murzin, D. Y. Catalytic Transformations of Citral in a Continuous Flow over Bifunctional Ru-MCM-41 Extrudates. *Catal. Sci. Technol.* **2021**, *11*, 2873−2884.

(21) Deliy, I. V.; Danilova, I. G.; Simakova, I. L.; Zaccheria, F.; Ravasio, N.; Psaro, R. Tuning Selectivity through the Support in the Hydrogenation of Citral over Copper Catalysts. In *Catalysis of Organic Reactions, Book Series: Chemical Industries*; Prunier, M. L., Ed.; CRC Press: Boca Raton, Florida, USA, 2009; Vol. *123*, pp 87−92.

(22) McKeown, D. A.; Post, J. E.; Etz, E. S. Vibrational Analysis of Palygorskite and Sepiolite. *Clays Clay Miner.* **2002**, *50*, 667−680.

(23) Vajglová, Z.; Navas, M.; Mäki-Arvela, P.; Eränen, K.; Kumar, N.; Peurla, M.; Murzin, D. Y. Transformations of Citral over Bifunctional Ru-H-Y-80 Extrudates in a Continuous Reactor. *Chem. Eng. J.* **2022**, *429*, No. 132190.

(24) Murzin, D. Yu. *Engineering Catalysis*; De Gruyter: Berlin, Boston, 2020; pp 1−414.

(25) Vajglová, Z.; Kumar, N.; Mäki-Arvela, P.; Eränen, K.; Peurla, M.; Hupa, L.; Murzin, D. Yu. Effect of Binders on the Physicochemical and Catalytic Properties of Extrudate-Shaped Beta Zeolite Catalysts for Cyclization of Citronellal. *Org. Process Res. Dev.* **2019**, *23*, 2456−2463.

(26) Vajglová, Z.; Kumar, N.; Mäki-Arvela, P.; Eränen, K.; Peurla, M.; Hupa, L.; Nurmi, M.; Toivakka, M.; Murzin, D. Yu. Synthesis and Physicochemical Characterization of Shaped Catalysts of Beta and Y

Zeolites for Cyclization of Citronellal. *Ind. Eng. Chem. Res.* **2019**, *58*, 18084−18096.
(27) Vajglová, Z.; Kumar, N.; Peurla, M.; Eränen, K.; Mäki-Arvela, P.; Murzin, D. Yu. Cascade Transformations of (±)-Citronellal to Menthol over Extruded Ru-MCM-41 Catalysts in a Continuous Reactor. *Catal. Sci. Technol.* **2020**, *10*, 8108−8119.
(28) Sing, K. S. W.; Everett, D. H.; Haul, R. A. W.; Moscou, L.; Pierotti, R. A.; Rouquerol, J.; Siemieniewska, T. Reporting Physisorption Data for Gas/Solid Systems with Special Reference to the Determination of Surface Area and Porosity (Recommendations 1984). *Pure Appl. Chem.* **1985**, *57*, 603−619.
(29) Beck, J. S.; Vartuli, J. C.; Roth, W. J.; Leonowicz, M. E.; Kresge, C. T.; Schmitt, K. D.; Chu, C.-T.-W.; Olson, D. H.; Sheppard, E. W.; McCullen, S. B.; Higgins, J. B.; Schlenker, J. L. A New Family of Mesoporous Molecular Sieves Prepared with Liquid Crystal Templates. *J. Am. Chem. Soc.* **1992**, *114*, 10834−10843.
(30) Vajglová, Z.; Kumar, N.; Peurla, M.; Hupa, L.; Semikin, K.; Sladkovskiy, D. A.; Murzin, D.Yu. Effect of the Preparation of Pt-Modified Zeolite Beta-Bentonite Extrudates on Their Catalytic Behavior in *n*-Hexane Hydroisomerization. *Ind. Eng. Chem. Res.* **2019**, *58*, 10875−10885.
(31) Kubička, D.; Kumar, N.; Venäläinen, T.; Karhu, H.; Kubičková, I.; Österholm, H.; Murzin, D. Yu. Metal- Support Interactions in Zeolite-Supported Noble Metals: Influence of Metal Crystallites on the Support Acidity. *J. Phys. Chem. B.* **2006**, *110*, 4937−4946.
(32) Özcan, A.; Kalipcilar, H. Preparation of Zeolite A Tubes from Amorphous Aluminosilicate Extrudates. *Ind. Eng. Chem. Res.* **2006**, *45*, 4977−4984.
(33) Vajglová, Z.; Simakova, I. L.; Eränen, K.; Mäki-Arvela, P.; Kumar, N.; Peurla, M.; Tolvanen, S.; Efimov, A.; Hupa, L.; Peltonen, J.; Murzin, D. Yu. The Physicochemical and Catalytic Properties of Clay Extrudates in Cyclization of Citronellal. *Appl. Catal., A* **2022**, *629*, No. 118426.
(34) Vajglová, Z.; Kumar, N.; Peurla, M.; Hupa, L.; Semikin, K.; Sladkovskiy, D. A.; Murzin, D. Yu. Deactivation and Regeneration of Pt-Modified Zeolite Beta−Bindzil Extrudates in *n*-Hexane Hydroisomerization. *J. Chem. Technol. Biotechnol.* **2021**, *96*, 1645−1655.
(35) Plößer, J.; Lucas, M.; Claus, P. Highly Selective Menthol Synthesis by One-Pot Transformation of Citronellal Using Ru/H-BEA Catalysts. *J. Catal.* **2014**, *320*, 189−197.
(36) Mertens, P.; Verpoort, F.; Parvulescu, A. N.; de Vos, D. Pt/H-Beta Zeolites as Productive Bifunctional Catalysts for the One-Step Citronellal-To-Menthol Conversion. *J. Catal.* **2006**, *243*, 7−13.
(37) Yongzhong, Z.; Yuntong, N.; Jaenicke, S.; Chuah, G. K. Cyclisation of Citronellal over Zirconium Zeolite Beta - a Highly Diastereoselective Catalyst to (±)-Isopulegol. *J. Catal.* **2005**, *229*, 404−413.
(38) Plößer, J.; Lucas, M.; Wärnå, J.; Salmi, T.; Murzin, D. Yu.; Claus, P. Kinetics of the One-Pot Transformations of Citronellal to Menthols on Ru/H-BEA Catalysts. *Org. Process Res. Dev.* **2016**, *20*, 1647−1653.
(39) Hughes, R. *Deactivation of Catalysts*; Academic Press: London, 1984; pp 1−265.
(40) Ostrovskii, N. M. General Equation for Linear Mechanisms of Catalyst Deactivation. *Chem. Eng. J.* **2006**, *120*, 73−82.
(41) Haario, H. *Modest 6.0 - a User's Guide*; ProfMath: Helsinki, Finaland, 2001.
(42) Zhivonitko, V. V.; Vajglová, Z.; Mäki-Arvela, P.; Kumar, N.; Peurla, M.; Murzin, D. Yu. Diffusion Measurements of Hydrocarbons in Zeolites with Pulse-Field Gradient Nuclear Magnetic Resonance Spectroscopy. *Russ. J. Phys. Chem. A.* **2021**, *95*, 547−557.
(43) Vajglová, Z.; Kumar, N.; Peurla, M.; Peltonen, J.; Heinmaa, I.; Murzin, D. Yu. Synthesis and Physicochemical Characterization of Beta Zeolite-Bentonite Composite Materials for Shaped Catalysts. *Catal. Sci. Technol.* **2018**, *8*, 6150−6162.
(44) Azkaar, M.; Mäki-Arvela, P.; Vajglová, Z.; Fedorov, V.; Kumar, N.; Hupa, L.; Hemming, J.; Peurla, M.; Aho, A.; Murzin, D. Yu. Synthesis of Menthol from Citronellal over Supported Ru- and Pt-Catalysts in Continuous Flow. *React. Chem. Eng.* **2019**, *4*, 2156−2169.

https://doi.org/10.1021/acs.oprd.1c00435
Org. Process Res. Dev. 2022, 26, 387−403